© 2020. Published by The Company of Biologists Ltd | Journal of Experimental Biology (2020) 223, jeb232702. doi:10.1242/jeb.232702

RESEARCH ARTICLE

Differential tissue stiffness of body column facilitates locomotion of *Hydra* on solid substrates

Suyash Naik[1,2,*], Manu Unni[1,*], Devanshu Sinha[2], Shatruhan Singh Rajput[2], Puli Chandramouli Reddy[1], Elena Kartvelishvily[3], Inna Solomonov[4], Irit Sagi[4], Apratim Chatterji[2], Shivprasad Patil[2,‡] and Sanjeev Galande[1,‡]

ABSTRACT

The bell-shaped members of the Cnidaria typically move around by swimming, whereas the *Hydra* polyp can perform locomotion on solid substrates in an aquatic environment. To address the biomechanics of locomotion on rigid substrates, we studied the 'somersaulting' locomotion in *Hydra*. We applied atomic force microscopy to measure the local mechanical properties of *Hydra*'s body column and identified the existence of differential Young's modulus between the shoulder region versus rest of the body column at 3:1 ratio. We show that somersaulting primarily depends on differential tissue stiffness of the body column and is explained by computational models that accurately recapitulate the mechanics involved in this process. We demonstrate that perturbation of the observed stiffness variation in the body column by modulating the extracellular matrix polymerization impairs the 'somersault' movement. These results provide a mechanistic basis for the evolutionary significance of differential extracellular matrix properties and tissue stiffness.

KEY WORDS: Biomechanics, Extracellular matrix, Tissue rheology, Atomic force microscopy

INTRODUCTION

Locomotion enables organisms to move from one place to another. The ability to move evolved very early in life forms, which accorded several advantages to the organisms. Locomotion offers exploration opportunities for food and water sources, mates, niches and, more importantly, escaping predators. Morphological diversity and tissue type innovations facilitated in the evolution of various means of locomotion in different organisms. The organisms that use specialized appendages and body oscillations to propel themselves are often known to share common biomechanical principles (Biewener, 1990; Gray, 1933; Alexander, 2003). While unicellular organisms use dedicated organelles such as cilia, flagella or pseudopodia, multicellular organisms exhibit a complex system of coordination among specific cell types to achieve locomotion (Bray, 2000). Although organisms from phyla such as Ctenophora and sponges are capable of locomotion involving coordination of their multicellular body, they do not possess specialized tissues, unlike the more complex eumetazoans (Bond and Harris, 1988; Matsumoto, 1991). Basal metazoans evolved two types of locomotion: fluid dependent and substrate dependent. Cnidarians have acquired the ability to perform coordinated locomotion both in water and on solid substrates and are the earliest phylum to have evolved differentiated neuronal/muscular tissues and extracellular matrix properties (Bode, 1996; Bode et al., 1990; Dupre and Yuste, 2017).

Cnidarians typically have two different types of body structures, viz. the medusa and the polyp forms (Galliot, 2000). The medusal organisms such as jellyfish perform the movement with the help of thrust or pull of fluids using the umbrella, and hence are dependent on the mechanics of fluids (Gemmell et al., 2015; Anderson and DeMont, 2000). The direction of movement can be controlled by directing the fluid flow with the help of muscles (Anderson and DeMont, 2000). *Hydra* is a cnidarian polyp lacking the medusal stage in its life cycle. It has a very slender yet extremely flexible body column, with equally flexible tentacles at the oral end. The flexibility of *Hydra* is primarily due to its unique extracellular matrix composition (Deutzmann et al., 2000). The more complex modes of locomotion in *Hydra* utilize the neuromuscular system. The muscular cells in the two germ layers are oriented orthogonally with respect to each other, which helps in controlling both the length and the radial width of the organism (Aufschnaiter et al., 2017). These muscular cells are controlled by different neural circuits to achieve a range of coordinated behavioral activities (Dupre and Yuste, 2017; Han et al., 2018; Davis et al., 1968). This ability of *Hydra* to coordinate contraction and relaxation helps the polyp to perform a range of movements such as swaying, looping and somersaulting (Trembley, 1744).

Here, we focused on *Hydra's* somersault, which involves coordinated movements of different body parts. It includes adhering to the substrate with the tentacles for traction. The body is then moved around the head in a semi-circular arc with characteristic contractions and relaxations (Fig. 1). It is initiated by stretching the body column almost to double its length (stage 1, Fig. 1) and by attachment of the head to the substratum with the help of tentacles and hypostome (Trembley, 1744; Han et al., 2018). During this process, the region of the body column just below the head referred to here as the 'shoulder', is bent by almost 90 deg. The basal disc at the bottom of the foot is then released, relaxing the stretched body column and accentuating the bend in the shoulder (stages 2–3). The bend straightens out (or is released) to achieve an 'upside down' position of the body column perpendicular to the substratum (stages 4–6) (Fig. 1, Movie 1). The process is completed by bending the body column, followed by attachment of basal disc to a new position. Finally, the oral end pushes itself away with the help of tentacles, and the body attains the upright position.

[1]Department of Biology, Indian Institute of Science Education and Research, Pune 411008, India. [2]Department of Physics, Indian Institute of Science Education and Research, Pune 411008, India. [3]Electron Microscopy Unit, Weizmann Institute of Science, Rehovot 7610001, Israel. [4]Department of Biological Regulation, Weizmann Institute of Science, Rehovot 7610001, Israel.
*These authors contributed equally to this work

[‡]Authors for correspondence (sanjeev@iiserpune.ac.in; s.patil@iiserpune.ac.in)

S.N., 0000-0001-8421-5508; M.U., 0000-0001-7504-4073; D.S., 0000-0002-5770-6720; S.S.R., 0000-0002-0747-1505; P.C.R., 0000-0002-7732-0331; E.K., 0000-0001-5517-8429; I.S., 0000-0003-2486-1350; I.S., 0000-0001-5595-5515; A.C., 0000-0002-8493-8463; S.P., 0000-0002-3413-4109; S.G., 0000-0002-7251-1905

Received 6 July 2020; Accepted 3 September 2020

Journal of Experimental Biology (2020) 223, jeb232702. doi:10.1242/jeb.232702

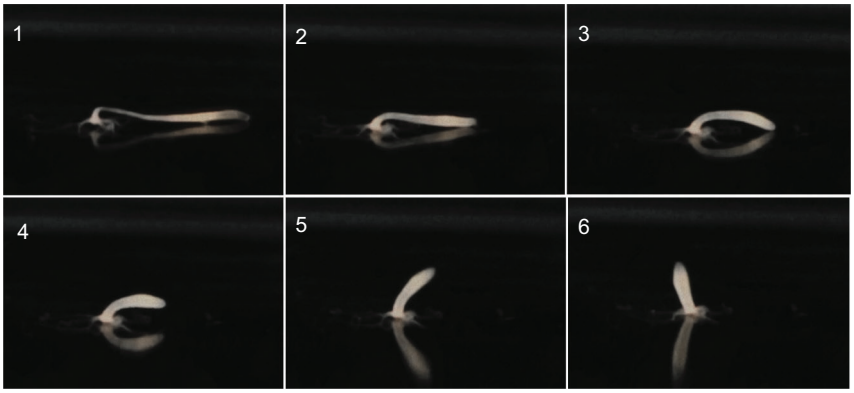

Fig. 1. The *Hydra* somersault. The stages of the *Hydra* somersault movement. In stage 1, the body column is stretched, and the tentacles hold on to the substrate. In stage 2, the basal end is released. In stage 3, the body column contracts. In stages 4 and 5, the body column is lifted.

To understand the biomechanics governing the somersault, we produced a spatially resolved elasticity profile of *Hydra*'s body column using an atomic force microscope. Atomic force microscopy (AFM) allows micro-elasticity maps of biological materials to be obtained (Tao et al., 1992). The profile obtained using AFM experiments was used to model *Hydra*'s body column in computer simulations to recapitulate part of the somersault movement. Further, we performed biological tests on *Hydra*'s ability to somersault when the differential tissue stiffness was perturbed by mechanical and chemical means. We observed that polyps with uniform stiffness along the body column lost their ability to perform a somersault. The extracellular matrix-mediated stiffness differential is presumably an ancient mechanism to accomplish specialized tissue function. In this study, we show that the extracellular matrix assumes a pseudo-skeletal property to help *Hydra* execute the somersaulting stunt.

MATERIALS AND METHODS

Hydra lines and culture

We used polyps from two strains of *Hydra vulgaris* Pallas 1766: *Hydra vulgaris* Ind-Pune and *Hydra vulgaris* AEP (Reddy et al., 2011; Martínez et al., 2010). *Hydra* polyps were cultured under standard conditions in glass bowls with *Hydra* medium containing KCl, NaCl, $MgSO_4{\cdot}7H_2O$, $CaCl_2{\cdot}7H_2O$ and Tris-HCl using the protocol described previously (Lenhoff, 2013). Both lines were maintained at 19°C and with a 12 h:12 h day:night cycle. Polyps were fed using freshly collected *Artemia* hatched in house. The medium was changed every day after feeding.

Measurement of *Hydra* tissue stiffness using AFM

Attaching a bead to the AFM lever

A tipless cantilever with a glass bead attached to its free end (stiffness ∼0.2 N m^{-1}) was used for AFM measurements. The diameter of the glass bead was 20 µm (Fig. 2A). The attachment was accomplished using the micromanipulation available via AFM. A small amount of UV-curable glue (Dymax 431) was spread on the coverslip. Using the servo control of the AFM, the end of the tipless lever was lowered onto the glue. A drop of glue was picked up on the lever and lowered again onto a bead. The lever was maintained under positive load and UV light was directed at the bead–lever assembly. After curing, the lever was pulled back from the surface along with the bead. The elastic modulus of the glue is 570 MPa, and it is not deformed while pushing on the tissue. Before performing force–distance measurements, the cantilever was calibrated using bovine serum albumin (BSA)-coated glass by thermal tuning.

Measurement of tissue stiffness using AFM

The *Hydra* body is unstable for mechanical measurements if it is not strongly adhered to the surface. A thin layer of BSA (10 mg ml^{-1}) was coated on the glass for strong adherence of the tissue. Young's modulus of various tissues typically ranges from 100 Pa to 1 MPa. The Young's modulus of glass is of the order of 10–100 GPa. The coating of BSA alters it to some extent. Fig. S1A shows the cantilever deflections for glass, BSA-coated glass and tissues from different parts along the body column. Assuming the glass–glass contact to be infinitely stiff compared with the glass–tissue contact – a reasonable assumption as it is 10,000 times stiffer – the slope of the curve in the contact region for glass and BSA-coated glass is nearly 1, implying no deformation. The slope of the curve on tissues is much less, suggesting a certain amount of deformation. We used glass–glass contact for calibration of deflection sensitivity; subtraction of cantilever deflection from the push given by the piezo extension yields deformation in the tissue. The force is calculated by multiplying the cantilever deflection by its stiffness. The force versus deformation curve is then fitted with the Hertz model:

$$F = \frac{E}{1-\nu^2}\left[\frac{a^2+R_s^2}{2}\ln\frac{R_s+a}{R_s-a} - aR_s\right], \quad (1)$$

$$\partial = \frac{a}{2}\ln\frac{R_s+a}{R_s-a},$$

where force F is measured by the cantilever holding the bead, which is pressed against the tissue; R_s is the bead radius; ∂ is the deformation in the tissue; E is Young's modulus; and ν is the Poisson ratio.

Hertz contact mechanics theory works for non-adhesive elastic contacts. It is important to establish that the pressing of the bead over the tissue conforms to this requirement. Fig. S1B shows a typical force–deformation measurement while both extending and retracting the bead over the tissue. For small loads (<1 nN), the extension and retraction curves do not show hysteresis, which indicates that the contact is non-adhesive and elastic.

Before AFM measurements, *Hydra* polyps were cultured and starved for a day to eliminate food material. They were relaxed with urethane (2% for 2 min; Sigma) and fixed immediately with glutaraldehyde (4%) for 30 min. The coverslip (diameter: 22 µm) was coated with a layer of BSA (10 mg ml^{-1}), and this layer was allowed to dry. The *Hydra* was placed on this layer, and a small amount of BSA was added to keep it from drying out. As the BSA dried, the connections formed between the *Hydra* and the surface by BSA were fixed using glutaraldehyde for 2 min, and water was

Journal of Experimental Biology (2020) 223, jeb232702. doi:10.1242/jeb.232702

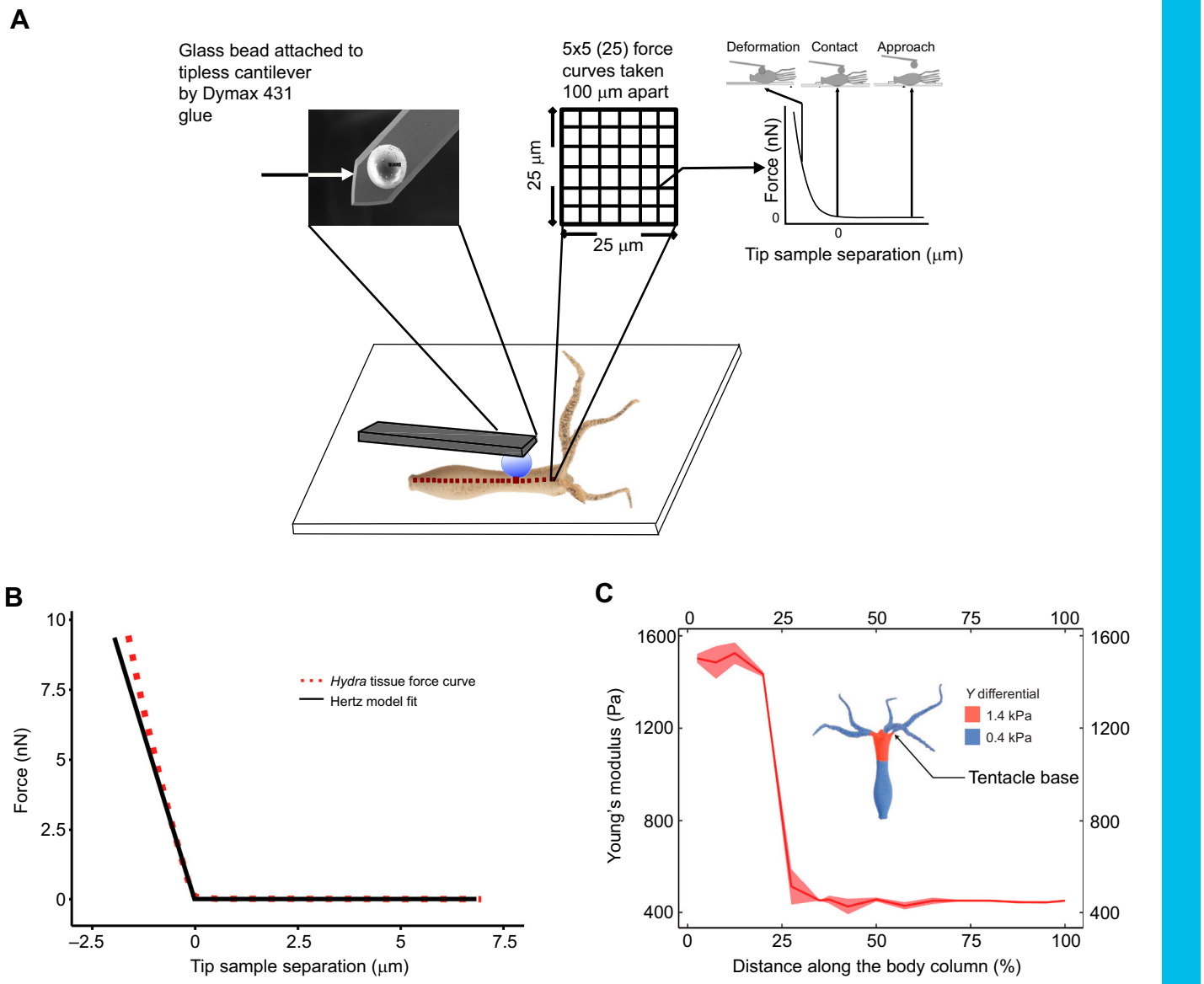

Fig. 2. Spatially resolved measurement of Young's modulus by force spectroscopy. (A) Schematic diagram of Young's modulus measurements along the *Hydra* body column. The *Hydra* was attached to a glass coverslip using BSA and glutaraldehyde, and measurements were recorded along the body column over grids separated by 100 μm. Each grid was 25 μm×25 μm with 25 force curves. The inset shows the image of a bead attached to a cantilever. (B) A typical force–distance curve used to fit the Hertz model to determine Young's modulus of a microcontact. The experimental data are shown as red dots, whereas the fit is depicted as a continuous black line. (C) The plot of variation in Young's modulus along the body column using atomic force microscopy (AFM). The distance from the tentacle end is plotted in units of percentage of total length, with 0% near the tentacles and 100% at the base. Force curves were taken at locations separated by 100 μm along the body column for three different polyps. The ribbon indicates the standard deviation of the mean over 25 measurements at each location. The inset is a schematic representation of variations in Young's modulus (*Y*) in different regions of *Hydra*. The top quarter of the body column is 3 times stiffer than the rest. See also Table S1.

added. The errors in the measurement of Young's modulus determine the width of the green rectangle (see below) used to depict the experimental measures of *Hydra*.

Measurement of the mass density of *Hydra*

The density of *Hydra* was measured by the following experiment. Tentacles were removed and the resulting *Hydra* body column was dropped in the water column in a vertical tube (height 2 m, diameter 5 cm). The body column attains terminal velocity, measured to be 0.003 m s^{-1}, and moves downwards horizontally without rotating or tumbling (Movie 6). After balancing the forces acting on a cylindrical body moving with terminal velocity in a fluid, we obtained:

$$\rho = \rho_0 + \frac{((4\pi\eta L)/\ln(L/D)) \times v}{V\boldsymbol{g}}, \quad (2)$$

where ρ is the density of *Hydra*; ρ_0 and η are the density and viscosity of water, respectively; *L*, is the length of the *Hydra* body column; *D* is the diameter of the body column; *V* is the volume of *Hydra*; and ***g*** is the acceleration due to gravity. We measured the length and diameter at five different locations across the body column of 10 different *Hydra* polyps. The errors in the measurement of *L* and *D* largely determine errors in estimating the density of

Journal of Experimental Biology (2020) 223, jeb232702. doi:10.1242/jeb.232702

Hydra from the measurements. The density of *Hydra* tissue is 1050 ±15 kg m^{-3}. This is 5±1.5% above the density of water. This error determines the height of the green rectangle (see below).

Videography and analysis of somersault

We recorded the motion of *Hydra* as it performs somersault movements and measured the statistics of somersaults with modification of native stiffness along the body column. We fabricated a glass tank (10×8×4.5 cm) and recorded the movement of *Hydra* as they detached from the surface, using a Nikon D-500 digital camera fitted with a 105 mm macro lens. For measurement of distances, a precise scale was kept in the tank. The videos were recorded at 25 frames s^{-1} for 20 min at a stretch. We assayed the propensity of *Hydra* to somersault after dropping them with a pipette into the tank. For ease of scoring, we only scored the number of times polyps stood upside-down as this is the first and most important step of the *Hydra* somersault. The normalization of the events was done by calculating the average and standardizing the values by comparison with the control. The videos were analyzed with Lightworks and Fiji software. For bending energy calculations in Fig. 3D, circles were fitted to the shoulder region of *Hydra* using Fiji software and the bend energy stored in the shoulder region was measured.

Extracellular matrix disruption

Hydra extracellular matrix has been shown to be dynamically regulated and important in regeneration as well. It has been seen before that amputation leads to a retraction of the extracellular matrix near the wound. This retraction is about 100 µm below the cut edge, and the extracellular matrix re-secretion takes about 24 h to complete (Sarras et al., 1991). We used this property of the extracellular matrix to physically perturb it upon nicking (partial cut/amputation) of the organism. Nicking was performed using the sharp bevel edge of a 31-gauge syringe needle and carefully controlled under a 10× dissection microscope. Adequate care was taken to ensure that the nick was always halfway through the body (incision up to half of the diameter of the polyp at the shoulder region) and perpendicular to the long body axis, such that the

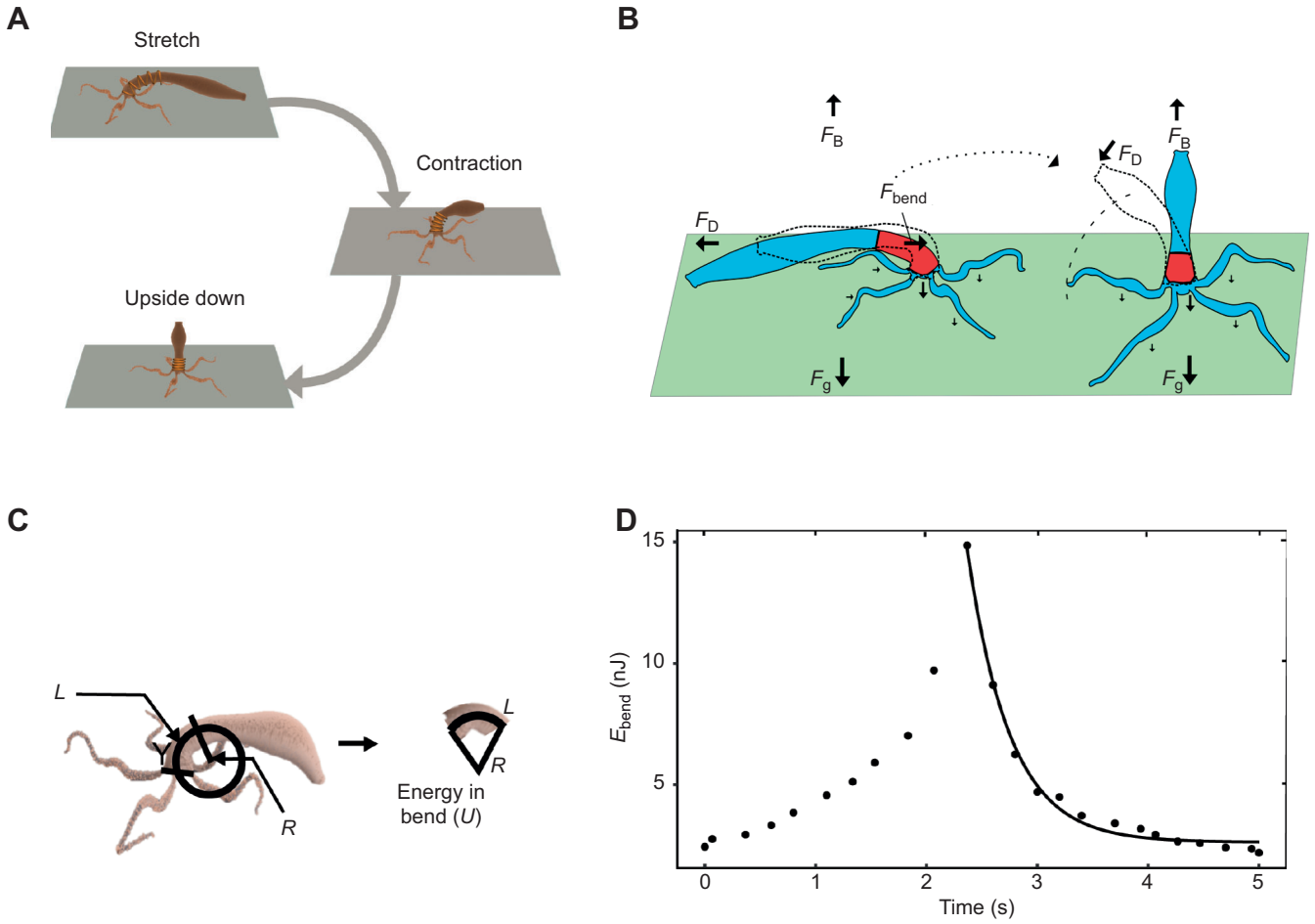

Fig. 3. Role of differential tissue stiffness in biomechanics of the *Hydra* somersault. (A) The stiffer shoulder region is depicted as a hypothetical spring. The *Hydra* and the deformations in this spring are shown as somersaults to reach the upside-down position. (B) The forces acting on the *Hydra* body column during the somersault. F_B represents the force of buoyancy in water acting against the gravitational force on the organism F_g. F_D is the drag force acting against the direction of motion. F_{bend} is the representation of the force acting on the head region due to energy stored in the bend. The changes in force as the *Hydra* goes from stage 1/2 (dotted outline) to stage 4 (dotted outline)/5 can be seen. (C) A schematic illustration of the calculation of energy stored in the bent shoulder (U; $U=YIL/2R^2$, where I is the second moment of inertia). The shoulder region of the *Hydra* was fitted to a circle to measure the radius of curvature (R) of the bend. The length (L) is 25% of the total length (the stiff region), and Y is the measured Young's modulus. (D) The progression of energy in the bend (E_{bend}) with time after release (t=0). E_{bend} first increases to a peak and then exponentially decays as the bend straightens to bring the body to an upside-down position. The continuous line represents the fit to a single exponent ($\tau\approx0.4$ s, n=1). See also Table S2.

severed part did not move away. We ensured that the head attached in the same place, and the wound had healed before carrying out videography of the somersaulting locomotion. This procedure led to a loss of extracellular matrix in a small region around the partial amputation. To assess the effect of loss of extracellular matrix in a particular region on the stiffness of the organism, we performed AFM-based measurements on polyps with the head partially cut. To assess the effect of localized extracellular matrix perturbation on the ability of *Hydra* to somersault, the polyps were videographed for somersaults 6 h post-amputation. Twenty polyps per experiment were used and a total of 3 experiments were performed, with no polyps reused for any experiments. These polyps were scored for 'events per *Hydra*' by counting the total number of occurrences of upside-down movement, termed 'events', from the time the polyps were dropped onto the container floor for a duration of 5 min; the number of events was then divided by the total number of polyps in the container to obtain the events per *Hydra* (Fig. 6).

2,2′-Dipyridyl (hereafter dipyridyl) is an inhibitor of lysyl oxidase (Siegel et al., 1970), an enzyme which crosslinks two adjacent fibrillar collagens to make bundles. Inhibition of lysyl oxidase prevents the components of the extracellular matrix from polymerizing. This has been shown before to be effective in inhibition of the *Hydra* extracellular matrix (Aufschnaiter et al., 2011). A concentration of 100 µmol l^{-1} has been shown to be effective in other strains of *Hydra*. To test the validity of this result, the behavior of *Hydra* under 50–200 µmol l^{-1} dipyridyl in *Hydra* medium was tested, and no physiological effects were detected until 175 µmol l^{-1} dipyridyl. For the partial amputation along with dipyridyl treatment experiments (see below), the organisms were pre-treated with 100 µmol l^{-1} dipyridyl for 12 h followed by nicking and further treatment with dipyridyl for 24 h. *Hydra* extracellular matrix is continuously cycling along the body column and replenished. Twenty polyps were used per experiment, and a total of three experiments were performed, with no polyps reused for any of the experiments. For the dipyridyl treatments (see below), dipyridyl was added to the *Hydra* medium at 100 µmol l^{-1}, and the medium was changed every 24 h. Stiffness measurements were performed using AFM on *Hydra* treated for 72 h to assess the effect of chemical extracellular matrix disruption on stiffness.

For comparison between effects of different experimental perturbations, we compared 20 animals for each condition in a biological replicate. Each biological replicate for an experimental perturbation was repeated with its respective control for three trials. The average number of somersaults for each condition was measured during a fixed time period. The averages for the replicates were compared with corresponding controls, and significance was measured using unpaired Student's *t*-test.

Scanning electron microscopy of *Hydra* tissue

Anaesthetized polyps (using 2% urethane for 2 min) were fixed using EM fixing solution [2.5% paraformaldehyde (Electron Microscopy Sciences, EMS), 2.5% glutaraldehyde (EMS) and 0.1 mol l^{-1} cacodylate buffer (Sigma)]. These polyps were then embedded in 5% agar and sectioned into 200 µm slices using a vibratome (Leica VT1200 S). The sections were then stained with 1% osmium tetroxide (Sigma), 1% tannic acid (EMS) and 1% uranyl acetate (EMS), and dehydrated by washing them serially with increasing concentrations of ethanol (30–100% ethanol). The sections were then dried at CO_2 critical point using a critical point dryer (Leica CPD030), then mounted on carbon tapes and sputter-coated with platinum. The coated samples were imaged using the Sigma 500 electron microscope (Zeiss).

Computational analysis

The experimentally observed value of the length of the *Hydra* body column is around 5 mm while its inner and outer radii are 0.05 mm and 0.1 mm, respectively. In our simulation, this is modelled as a hollow cylindrical tube of diameter of a=1 simulation units (s.u.) and length L_0=30a (see Table 1).

The stretched elastic body of *Hydra* is characterized by its Young's modulus Y, stored elastic energy E, length L, cross-sectional area A (determined from its inner and outer radii) and its mass $M=\sum m_i$, where m_i is the mass of the ith bead. Five hundred such beads are arranged in rings to form the cylinder. The viscous drag due to liquid surrounding the *Hydra* is characterized by the drag coefficient Γ. These parameters are combined to form a dimensionless parameter D:

$$D = \frac{\Gamma L^{3/2}}{E}\sqrt{\frac{YA}{M}}. \tag{3}$$

Substituting $k_{\text{eff}}=YA/L$, which is essentially replacing the Young's modulus by the stiffness constant of an equivalent spring, gives us:

$$D = \frac{\Gamma L^{2}}{E}\sqrt{\frac{k_{\text{eff}}}{M}}. \tag{4}$$

We estimated the following parameters.

Elastic energy (*E*)

The experimentally measured Young's modulus was around 1000 Pa. Assuming a linear stress (σ)–strain (ε) relationship, $\sigma=Y\varepsilon$, the stored elastic energy per unit volume is given by the integral of the stress–strain curve. The energy stored in volume V at a strain of ε=1 is:

$$E = V\int_0^1 \sigma \mathrm{d}\varepsilon = V\int_0^1 Y\varepsilon \mathrm{d}\varepsilon = \frac{YV}{2}. \tag{5}$$

Using experimentally measured parameters of *Hydra*, the stored elastic energy is:

$$E = \frac{YV}{2} = \frac{10^3\text{Pa}\times\pi(1^2-0.05^2)\times10^{-8}\text{m}\times5\times10^{-3}}{2} \approx 6\times10^{-8}\text{J}. \tag{6}$$

Table 1. Simulation units of physical quantities

Dimension	Simulation units	SI units
Length (L)	a=1	0.17×10^{-3} m
Mass (M)	m_i=1	2×10^{-10} kg
Time (T)	τ=1	0.91×10^{-3} s

Stoke's friction coefficient for a cylinder (Γ)

The diameter to length ratio (d/L) of *Hydra* is a small fraction and can be approximated as a long thin cylindrical tube (Akhtar et al., 2011; Dhont, 1996). The drag coefficient under this approximation is divided into two parts: one parallel to the cylinder axis (running along its length), which we call $\Gamma^{\parallel}$, and the other perpendicular to the axis $\Gamma^{\perp}$. The expressions for these coefficients are:

$$\Gamma^{\parallel} = \frac{2\pi\eta L}{\ln(L/d)}, \tag{7}$$

$$\Gamma^{\perp} = \frac{4\pi\eta L}{\ln(L/d)}, \tag{8}$$

where L and D are the length and diameter of *Hydra* body, respectively; and η is the viscosity of water. Here, $\Gamma^{\parallel}=\Gamma^{\perp}/2$. As these values do not differ by an order of magnitude, we take their average value as the drag coefficient:

$$\Gamma = \frac{\Gamma^{\parallel} + \Gamma}{2} = \frac{3\pi\eta L}{\ln(L/d)}. \tag{9}$$

Setting the viscosity of water as 10^{-3} Pa, L=5×10^{-3} m and d=10^{-4} m, we get Γ=1.2×10^{-5} N s m^{-1}.

Mass (*M*)

We measured *Hydra*'s body to have a mass density of 1050 kg m^{-3}, and its mass can be estimated from its volume multiplied by its density as about 10^{-7} kg.

Stiffness constant of equivalent spring (k_{eff})

We calculated k_{eff} as:

$$k_{\mathrm{eff}} = \frac{YA}{L} = \frac{10^3\mathrm{Pa} \times \pi(r_{\mathrm{outer}}^2 - r_{\mathrm{inner}}^2)}{5 \times 10^{-3}\mathrm{m}^3} \approx 0.5 \times 10^{-2}\mathrm{N\,m^{-1}}. \tag{10}$$

Using these values, the theoretically estimated value of the dimensionless parameter D is:

$$D = \frac{\Gamma L^2}{E}\sqrt{\frac{k}{M}} = \frac{(1.2 \times 10^{-5})(5 \times 10^{-3}\mathrm{m})^2}{6 \times 10^{-8}\mathrm{J}}\sqrt{\frac{0.5 \times 10^{-2}\mathrm{N\,m^{-1}}}{10^{-7}\mathrm{kg}}} \approx 1.1. \tag{11}$$

The simulation parameters were chosen such that this dimensionless quantity remains unchanged when calculated using the simulation units. The choice of a stiffness constant fixes the stored elastic energy of the system. Using the effective stiffness value of 20 s.u., the stored energy can be calculated as $\frac{1}{2}k_{\mathrm{eff}}(\Delta x_{\mathrm{sim}})^2$. Given a neutral length of the simulation *Hydra* of 30 s.u., stretching to twice its length results in Δx_{sim}=30 s.u. Using these values along with the simulation mass as 500 s.u. (each bead being assigned a mass of 1 unit, with 500 beads forming the cylinder), we get:

$$D_{\mathrm{sim}} = \frac{\Gamma_{\mathrm{sim}} L_{\mathrm{sim}}}{E_{\mathrm{sim}}}\sqrt{\frac{k_{\mathrm{eff,sim}}}{M_{\mathrm{sim}}}} = 0.02 \times \Gamma_{\mathrm{sim}} = D = 1.1. \tag{12}$$

Solving for Γ_{sim}, the value of Stoke's coefficient for the cylinder in simulation units is Γ_{sim}=55 s.u. As our mass–spring system consists of 500 beads, each bead can be assigned a viscous Stoke's coefficient of Γ_{sim}/(no. of beads)=55/500 s.u.=0.11 s.u.

Time

We can construct a unit of time using the drag coefficient Γ, neutral length of the *Hydra* L_0 and the elastic energy stored upon a strain of ε=1 as:

$$\tau = \frac{\Gamma L^2}{E}. \tag{13}$$

Having fixed the Stoke's coefficient in the previous step, we arrive at a correspondence between the real time units and the simulation time units. As all the parameters are known:

$$\tau_{\mathrm{sim}} = \frac{\Gamma_{\mathrm{sim}} L_{\mathrm{sim}}^2}{E_{\mathrm{sim}}} = \frac{55 \times 30^2}{9000} = 5.5\,\mathrm{s.u.} \tag{14}$$

This must be equal to the real time units:

$$\tau = \frac{\Gamma L^2}{E} = \frac{1.2 \times 10^{-5}\mathrm{N\,s\,m^{-1}} \times (5 \times 10^{-3}\mathrm{m})^2}{6 \times 10^{-8}\mathrm{J}} = 5 \times 10^{-3}\mathrm{s}. \tag{15}$$

Comparing these two yields:

$$1\ \mathrm{s} = \frac{5.5}{5 \times 10^{-3}} = 1.1 \times 10^3\ \mathrm{s.u.} \tag{16}$$

We confirmed that keeping the quantity $\Gamma_{\mathrm{sim}}L_{\mathrm{sim}}^2/E_{\mathrm{sim}}$ constant yields the same relaxation behavior of the model.

$E_{\mathrm{threshold}}$

We estimated the threshold energy required to overcome both viscous drag and gravitation by first performing a continuous integration of the drag force (per bead) along the path traced by each bead as the model *Hydra* evolves in time from its configuration at the end of the contraction to its final configuration (inverted position). The sum of all such integrals (over all 500 beads i) gives the total drag energy dissipated from the initial (after contraction) to the final configuration. We add to this the gravitational potential energy of the final configuration ($\sum m_i \boldsymbol{g} h_i$), the sum over the gravitational potential energies of each bead in their final configuration. $E_{\mathrm{threshold}}$ can then be written as:

$$E_{\mathrm{threshold}} = \sum_{i}^{500} \int_{t_c}^{t_{\mathrm{final}}} \gamma v_i(t)\mathrm{d}s_i(t) + \sum_{i}^{500} m_i \boldsymbol{g}' h_i, \tag{17}$$

where i is the bead index; t_c and t_{final} are the time at the end of the contract step and the end of somersault when the model *Hydra* is in the inverted position; γ is the damping coefficient; and $\mathrm{d}s_i(t)$ is the incremental displacement of the ith bead as a function of time. $\boldsymbol{g}'$ is the effective gravitational acceleration used for calculation. It is only a small fraction of the actual gravitational acceleration ($\boldsymbol{g}$) to account for buoyancy resulting from the density difference between *Hydra* tissue and water.

RESULTS

Measurement of local variation in tissue stiffness

Multicellular organisms use spatially differentiated tissue types, such as the exoskeleton in invertebrates or the musculoskeletal system in vertebrates, to resist strain and sustain traction during locomotion (Biewener, 1990; Dickinson et al., 2000). These

specialized tissues exhibit differential stiffness properties that facilitate locomotion. It was not known whether *Hydra* possesses any tissue elasticity-dependent mechanisms to assist its locomotion. We used AFM for the first time to produce a spatially resolved map of tissue elasticity in *Hydra*. As shown in Fig. 2A, we attached glass beads (diameter 20 µm) to cantilevers and carefully allowed the bead to touch the *Hydra* body, which was positioned on a BSA-coated coverslip. With the help of servo control, we record the force curves in which the load on the tissue and its deformations were measured by recording the cantilever deflection and substrate displacement. The force curves were taken at locations separated by 100 µm along the body column. At each location, we collect 25 force curves over a 5×5 grid and an area of 25 µm×25 µm. A total of three polyps were used (n=3) in each experiment for stiffness measurement. Using Hertz contact mechanics, we estimated the Young's modulus from each force curve, and the average was then calculated for each location (for further details, see Fig. S1A,B). Fig. 2B shows a typical force curve and fit using the Hertz model. Fig. 2C shows the elasticity profile acquired using these measurements. We observed higher stiffness in the region below the base of the tentacles, which extended up to 25% of the length of the body column, referred to as the shoulder region. The shoulder region was nearly 3-fold stiffer (Y=1480±20 Pa) than the rest of the body (Y=450±6 Pa). For tentacles, Y=378±11 Pa (Fig. S1C). These measurements revealed a steep drop in stiffness at the junction of the shoulder and the rest of the body column (Fig. 2C; Fig. S1D). The entire set of measurements was repeated for three different polyps (Fig. S1D).

In *Hydra*, the novel sharp change in tissue elasticity along the body column leads to mechanically distinct behavior. Deformations under similar forces would be larger in the body column than in the shoulder region and the restorative forces would be lower in the body column. The observation that *Hydra*'s shoulder is 3 times stiffer suggests that this allows the shoulder to store larger mechanical energy for a given bend. The shoulder region can be viewed as a stiff spring with a high bending rigidity due to its higher Young's modulus (Fig. 3A). This is interesting in the context of the somersault, as initially the deformation is seen in the body column and the shoulder region is deformed in the later stages of the movement (Fig. 1). We reasoned that the deformation in the neck generates a force F_{bend}, which is used to overcome forces resulting from gravity (F_g), buoyancy (F_B) and viscous drag (F_D). Fig. 3B shows a hypothetical force diagram to better illustrate the forces acting on the organism as the somersault occurs.

Although the somersault is an active movement, the observed variation in elasticity points to a possible mechanism to store and release mechanical energy, which is adopted by animal movement to minimize metabolic costs (Roberts, 2016). Careful analysis of the somersault reveals that after release from the basal end, the bend in the shoulder becomes pronounced. To overcome the viscous and gravitational force on the body column while standing upside down, the energy stored in the bent shoulder is utilized. We analyzed each frame of the somersault to estimate the stored energy in the bend (E_{bend}) and its progression in time after release from the basal end. The radii of circles measured at different times were used to calculate the bending energy U using $U=YIL/2R^2$, where Y is the Young's modulus of the shoulder region (stiffer spring), I is the second area moment of inertia $I=\int r^2 dA=\pi(r_1^4-r_2^4)$, L is the length of the shoulder region in *Hydra* (25% of body column), R is the radius of the circle fitted to the shoulder region, r is the perpendicular distance of an elemental area dA along the axis of bending, and r_1 and r_2 are the outer and inner radii of the *Hydra* body column, respectively. The change in energy was observed from the point of detachment from the substrate to the final vertical native state of the *Hydra*. We computed E_{bend} using Young's modulus measured using AFM and radius of curvature R obtained by fitting circles to the shoulder region in each frame of the captured video as shown in Fig. 3C. Fig. 3D depicts the progression of energy in the bent shoulder, E_{bend}, with time. E_{bend} initially increased with time, suggesting a transfer of energy from stretch to the bend. This indicated that after the release, transferring part of the initial mechanical energy into the bend might serve as a crucial step in the biomechanics of the *Hydra* somersault. *Hydra* lacking a mechanism to facilitate such a transfer to optimize the peak in E_{bend} may not have sufficient energy to work against gravity and complete the somersault. After reaching the peak, E_{bend} is used to work against gravity and viscous resistance to reach the upside-down position and is expended at an exponential rate (Fig. 3D). A single exponent is characteristic of a bent elastic beam relaxing its stress in a viscous environment (Barnes et al., 1989) and indicates that the motion after release is predominantly governed by passive mechanics. The hypothesis that part of the somersault in which the body is lifted upside down is passive was further investigated using computer simulations and biological experiments (see below).

Simulations predict the importance of tissue stiffness variation in somersaults

To gain insight into the role of the observed variation in tissue stiffness in facilitating an efficient transfer of mechanical energy to bend, we simulated the part of the somersault which is passive and is depicted in Fig. 1. We modeled the tubular body of *Hydra* by a suitable network of 50 rings, each with 10 beads. These rings were stacked together to form an elastic cylinder of length L, as shown in Fig. 4A. The individual springs have spring constant k. The effective spring constant of the cylinder is k_{eff}. We observed that k_{eff} varied linearly with k (Fig. S2A,B). The experimentally measured mass, length and Young's modulus of *Hydra* were used to convert simulation units of m, L and k_{eff} into physical units. To model the experimentally observed stiffness variation along the *Hydra* body column, spring constants k of individual springs in the shoulder region were chosen to be α times the remainder of the body column (Fig. 4A). In simulations, for the same amount of initial energy when the cylinder is stretched (30 nJ), α was varied from 1, which indicates uniform stiffness, to a relatively large value of 30 to investigate the importance of spatial variation in tissue stiffness for the mechanics of somersault. Additionally, to truly represent the physical environment, we included viscous drag, the force of gravity and buoyancy on each bead of the model *Hydra* (Fig. S3).

To model the role of elasticity in energy transfer from stretch to bend (Fig. 3D), we stretched the cylinder and fixed the two rings at the ends nearly horizontally with strain ε=0.8 and 0.2. This range of strain values is typically seen in somersault videos. We then released the basal end, which has a lower stiffness. Qualitatively, the somersault in real *Hydra* compares well with simulations for α=3, which is observed in AFM experiments (see Fig. 4B). Interestingly, under uniform stiffness along the length of the cylinder (α=1), the model *Hydra* was unable to stand upside down after the release (Fig. 5A; Movie 2), suggesting that the observed variation in tissue stiffness plays an important role in completing the somersault.

The simulations indicated that before the release of the basal end, the potential energy stored in the shoulder for α=3 was lower than that for α=1. This was due to the comparatively larger stretch in the shoulder for α=1. However, after release, roughly 50% more energy was transferred to the shoulder region in the case of α=3 compared

Journal of Experimental Biology (2020) 223, jeb232702. doi:10.1242/jeb.232702

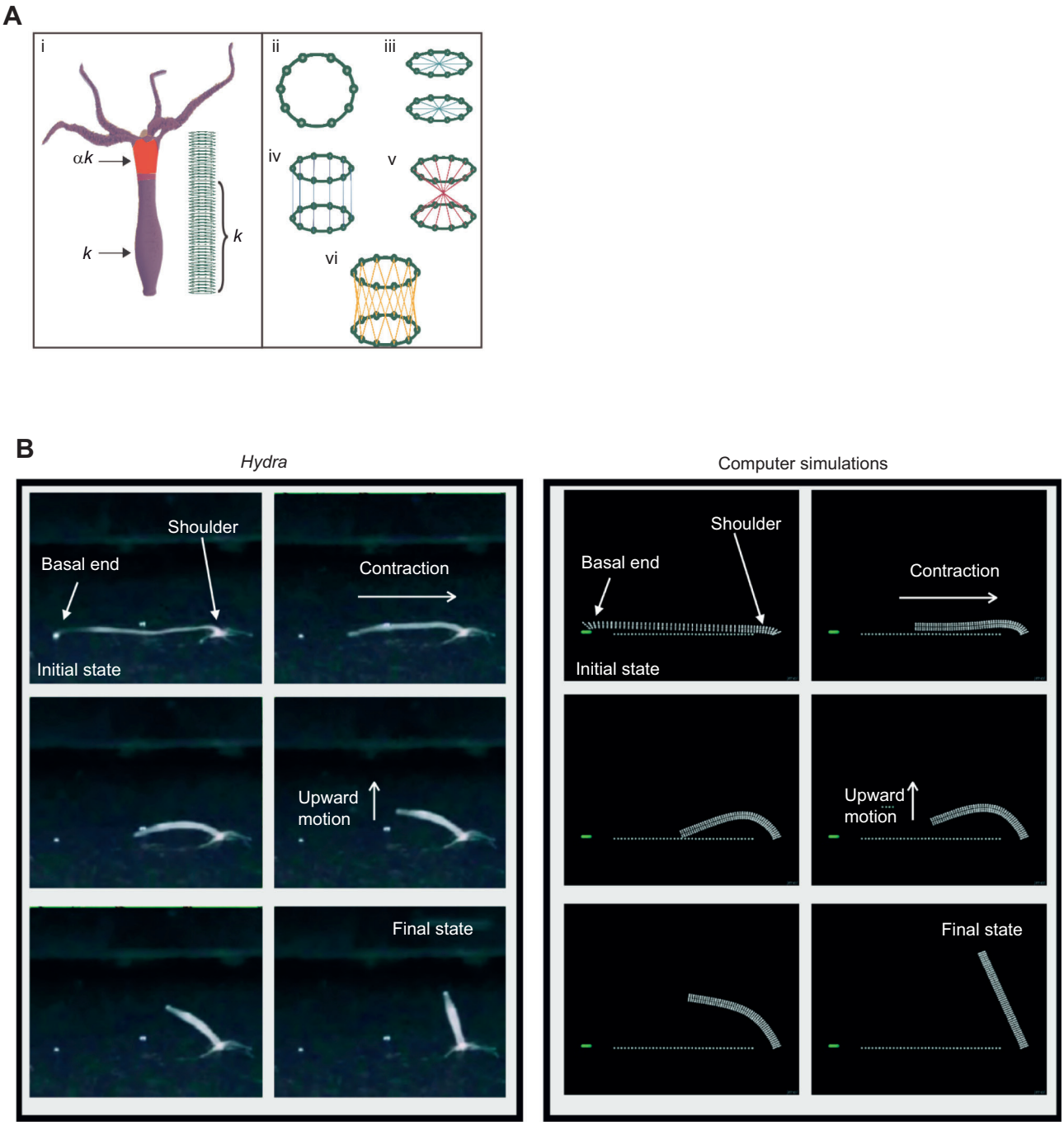

Fig. 4. Computer simulations can reproduce the somersault. (A) Modeling of the *Hydra* body column to represent various steps involved in the somersault movement. (i) An elastic cylinder comprising beads–springs was used to model the *Hydra* body column. The cylinder is a stack of 50 rings, each consisting of 10 beads of mass *m*. (ii–vi) Beads within the same ring and from adjacent rings are connected to each other with springs to maintain the circular cross-section (ii) and resist bending (iii), stretching (iv), torsion (v) and shear (vi). The effective spring constant k_{eff} of a quarter of the body length (shoulder) is kept at α times the rest. (B) Comparison of various experimentally recorded stages of the *Hydra* somersault with simulations. The simulations were performed by incorporating the experimentally observed variation in tissue stiffness. There are striking similarities between both the actual *Hydra* movement and its simulations.

with α=1. The end of the horizontal movement of the base signifies the end of the contraction. The stored energy in the shoulder region at the end of the contraction step is expended to overcome gravity and viscous drag. The energy threshold ($E_{threshold}$) required to stand upside down can be calculated (Fig. 5A). For α=1, the stored energy in the shoulder was below this threshold, and for α=3 it was above it. This suggested that if *Hydra* body column were to harbor uniform stiffness, then it would not be able to stand up (Fig. 5A). This result was robust with respect to different values of ε (Fig. S4A,B). It is important to note here that our model treated stage 4 of the somersault as passive. We were encouraged to model *Hydra*'s body column as a network of springs and beads because of our observation in Fig. 3B that the energy in the bend is expended in a passive manner to work against viscous and gravitational forces. Here, we focused on the energy transfer process and its utilization to stand upside down. The actual somersault, in its entirety, is a

Journal of Experimental Biology (2020) 223, jeb232702. doi:10.1242/jeb.232702

mixture of both active and passive processes and we simulated the passive stage alone. The broad inference that can be drawn from the simulations is that the differential stiffness aids in standing upside down. In particular, it was also suggested that the passive energy transfer facilitated by the differential tissue stiffness was a necessary condition for somersault and *Hydra* with uniform stiffness should not be able to rise upside down. This prediction from the simulations was then tested experimentally (see below).

To explain the physics behind the efficient energy transfer for α=3, we analyzed the simulation data. During contraction, the velocity difference between the shoulder and body column was larger for a model *Hydra* with non-uniform stiffness (α=3) compared with the uniform case (α=1). This generated more force on the shoulder region while the body column contracted. We calculated time-averaged longitudinal force on the 14th ring, which resides at the junction between the stiff shoulder and the labile body column (Fig. 5B). Clearly, the force was higher for α=3 than for α=1. The bend in the shoulder, in turn, received adequate energy for standing upside down. To find out the optimal variation of tissue stiffness for the highest possible energy transfer, we performed simulations for all values of α. Strikingly, force did not increase monotonically with α but exhibited a clear peak, indicating that a specific variation in tissue stiffness characterized by α was optimal for energy transfer in *Hydra* somersault and arbitrarily large values of α do not ensure effective energy transfer. Thus, the simulations indicated that the variation in tissue stiffness observed in the AFM measurements facilitates the somersault.

As the variation in tissue stiffness, characterized by α, facilitated efficient energy transfer from a stretch to a bend, which was used to overcome the hydrodynamic drag and the weight of body column due to the density difference ($\Delta\rho$), the successful completion of a somersault depends on $\Delta\rho$ and α. The experimentally measured mass density of *Hydra* is 5.0±1.5% higher than the density of water. We generated phase diagrams of $\Delta\rho$ versus α for a range of Young's modulus values. We observed that for extremely labile bodies (Y<10 Pa), the energy transferred from the stretched state to the bend was lower than the threshold and *Hydra* was unable to rise for all values of α (Fig. S5D). For extremely stiff bodies (Y>10 kPa), the energy required to stretch to 80% strain was large and the transferred energy was always above the threshold such that *Hydra* was always able to rise for all values of α (Fig. S5C). These two extremes are far from the experimentally observed stiffness and its variation in real *Hydra* tissue. Fig. 5C shows a phase diagram of $\Delta\rho$ and α at the experimentally observed values of Y. Note that in order to keep the amount of energy and strain fixed when the model *Hydra* was stretched, for α<3, Y for the body region was kept larger than 500 Pa. For α>3, the Y for the body region was kept smaller than 500 Pa. For Y=500 Pa throughout the body column, the *Hydra* was not able to rise and stood inverted if the tissue was 2.5% denser than water. The experimental measures of *Hydra*, $\Delta\rho$ and α lie inside the green rectangular shape in Fig. 5C.

The experimentally measured stiffness of *Hydra* tissue is likely to be an overestimate due to treatment with glutaraldehyde. It was difficult to quantify this effect in *Hydra*; however, the observed increase in Young's modulus as a result of this treatment on rat tail tendons quantified using AFM is nearly 50% (Hansen et al., 2009). We performed simulation runs to monitor the effect of such overestimates on the behavior observed in the phase plot of Fig. 5C. Fig. 5D shows a phase diagram in which Y for both shoulder and body column was halved compared with the experimentally observed values in our AFM measurements. The variation characterized by α was seen to be important in both cases (Fig. 5C,D). For the range of stiffness that was halved compared with the AFM measurements, *Hydra* with uniform stiffness was unable to lift its body column, even if it was 1% above the density of water (Fig. 5D). The phase diagram is robust with respect to strain and different initial energies stored in the stretch (Fig. 5C,D; Fig. S5A). This clearly indicates that a model *Hydra* with larger α, signifying an improved energy transfer, can lift itself even if it is heavy, which was described by a larger $\Delta\rho$. It is also interesting that the critical behavior for lifting the body column was observed in the phase plot of $\Delta\rho$ and α only for the range of tissue stiffness observed in real *Hydra*.

Modulation of extracellular matrix polymerization perturbs tissue stiffness variation, impairing the somersault

To identify the source of tissue stiffness and its differential, we hypothesized two possibilities, i.e. variation in the cell types or differences in the extracellular matrix composition. A recent report suggested that there is no difference in cellular stiffness in *Hydra* cells and hence we ruled out the possibility of a cellular contribution (Carter et al., 2016). Stiffness variation due to extracellular matrix composition could be tested by selectively disrupting physical properties of mesoglea without disrupting the chemical composition, avoiding the possibility of disturbing integrin–extracellular interactions. *Hydra* mesoglea (extracellular matrix) is a trilaminar porous structure which divides the two germ layers throughout the polyp and is in a perpetually stretched state (Sarras, 2012). Therefore, any lesion to the mesoglea leads to retraction of the mesoglea from the site of injury (Sarras, 2012; Shimizu et al., 2002). The outermost layer of the extracellular matrix is similar to the basement membranes consisting of cell-interacting extracellular matrix proteins such as collagen type IV and laminins (Sarras, 2012). The layer sandwiched by the basement membrane, called the interstitial matrix, is primarily made up of fibrillar collagens such as collagen type I, II, III and IV and hence can provide mechanical support to the polyp (Sarras, 2012).

Based on these properties, we devised physical and chemical perturbations to mitigate the stiffness of the extracellular matrix. In the physical method, we exploited the retractile property of the extracellular matrix to locally disrupt stiffness, which would sever the hypothetical 'spring' (Fig. 6A). In contrast, the chemical method used dipyridyl, a lysyl oxidase inhibitor, to inhibit polymerization of the newly secreted fibrillar collagen into fibrils in the extracellular matrix, therefore globally affecting the physical properties of newly synthesized extracellular matrix as it replaces old extracellular matrix without changing its composition (Fig. 6B) (Shimizu et al., 2002; Sarras et al., 1991; Siegel et al., 1970).

On two different sets of *Hydra* polyps, we partially lesioned the shoulder region and the middle of the body column, severing the extracellular matrix (n=20 polyps per experiment, n=3 experiments). Then, we recorded the somersaults performed 6 h after the lesion. This time point was chosen as it is sufficient time to heal the wound but not long enough to regain the stiffness around the lesion because the extracellular matrix is not fully regenerated (Sarras et al., 1991; Shimizu et al., 2002) (Fig. 6A; Movie 3). Further, the stiffness measurements using AFM revealed the loss of differential stiffness seen in the *Hydra* body column (Fig. S6A). Strikingly, the ability to perform somersaults was almost entirely lost when the lesion occurred in the shoulder region, whereas it remained unaffected when the lesion was in the body column (Fig. 6A). The polyps with a lesion in the shoulder were able to regain the ability to somersault after 36 h, a duration long enough to complete the regeneration of the extracellular matrix. Thus,

Journal of Experimental Biology (2020) 223, jeb232702. doi:10.1242/jeb.232702

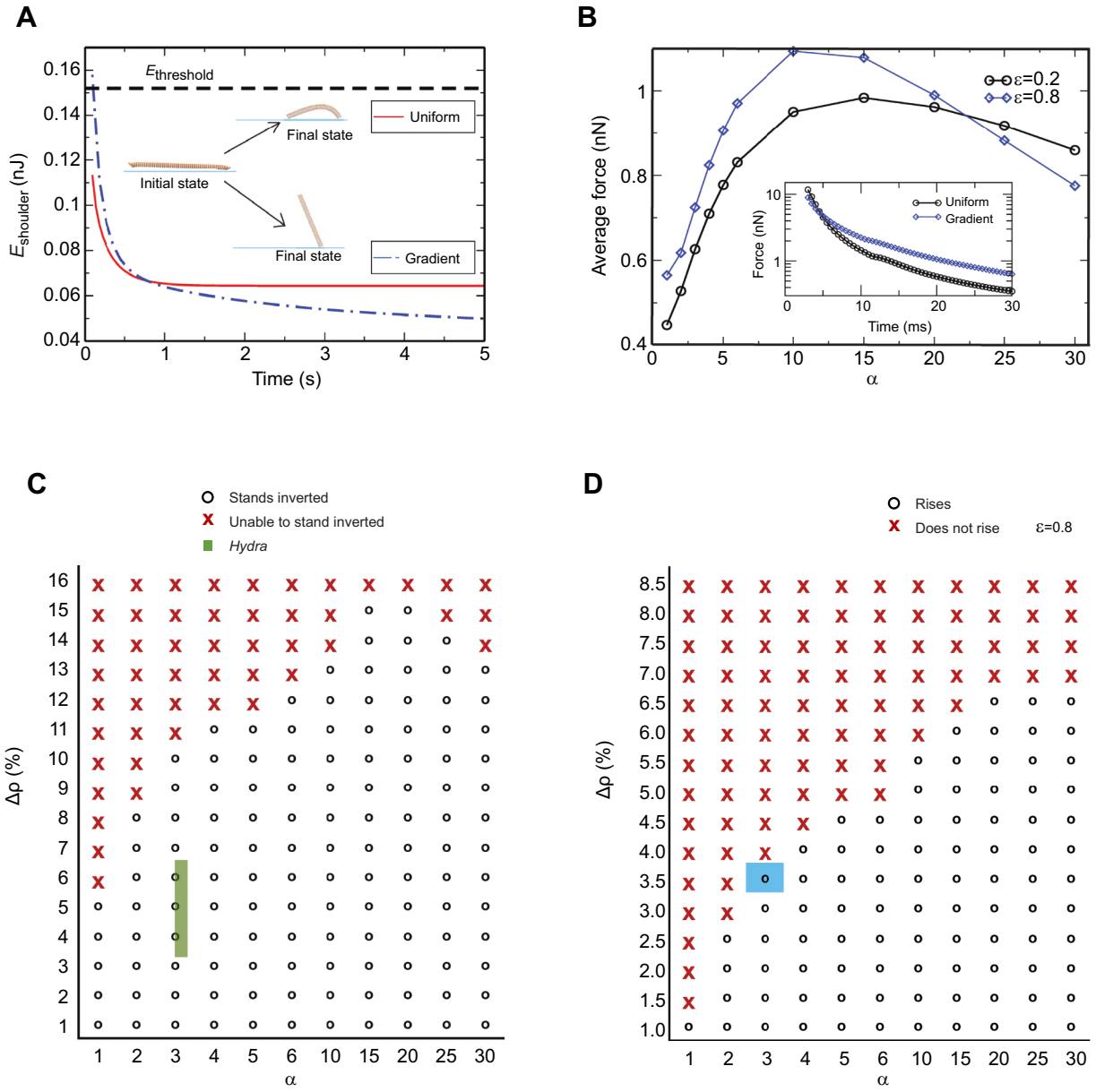

Fig. 5. Computer simulations unravel the significance of the differential in tissue stiffness for the somersault. (A) Plot of the energy in the shoulder region $E_{shoulder}$ versus time after the end of a contraction for strain ε=0.8. $E_{threshold}$ is the calculated minimum energy required to overcome gravity and viscous drag. At the end of a contraction, $E_{shoulder}$ is higher than $E_{threshold}$ for α=3 (stiffness differential seen in AFM experiments) and less than $E_{threshold}$ for α=1 (uniform stiffness). The simulation snapshots of the cylinder show its initial and final positions for α=1 and α=3. (B) The plot of time-averaged longitudinal force on the 14th ring, which is at the junction of the stiff shoulder and rest of the body column, with respect to α after the release. The force on this ring peaks at an intermediate value of α and does not increase monotonically. This indicates that arbitrarily large values of α do not facilitate the optimal energy transfer. The inset shows force versus time for α=3 and α=1 before the contraction is complete at ∼50–100 ms. Initially, the force is nearly the same in the two cases, but it becomes roughly double for α=3 at later times. (C) Phase diagram to describe the importance of tissue stiffness variation along the body column to overcome downward force on it due to a higher density of *Hydra* tissue compared with water. The region represented by crosses is the range of parameters for which model *Hydra* is unable to stand inverted after the release, and open circles represent the range for which it is able to stand inverted. The experimentally measured parameters of *Hydra* lie in the green rectangle in the phase space. The width and height of the rectangle represent experimental errors involved in estimating α and the mass density of *Hydra*, respectively. The initial strain ε is 0.8. (D) Phase diagram of the change in density (Δρ) and α with a Young's modulus that is half of experimentally observed value. The uniform stiffness (α=1) enables *Hydra* to lift the body column having a density difference of only 1% compared with water. The blue square denotes the lower bound of density of real *Hydra* tissue and α=3. The plot underscores the importance of variation in stiffness even if it is overestimated in AFM measurements as a result of glutaraldehyde treatment. See also Table S3.

elimination of the stiffness locally within the shoulder region resulted in an inability to perform the somersaults, underscoring the importance of the stiffness differential. The stiffness measurements using AFM revealed that the polyps treated with dipyridyl for 72 h exhibited uniform stiffness across the entire body column (Fig. S6B). This suggests that *Hydra* exploits the differential crosslinking of fibrillar collagen to generate tissues with varying degrees of elasticity. The ability to somersault was completely lost after 72 h of dipyridyl treatment, whereas the number of somersaults was reduced to half after 36 h of treatment (Fig. 6B; Movie 4) (*n*=20

Journal of Experimental Biology (2020) 223, jeb232702. doi:10.1242/jeb.232702

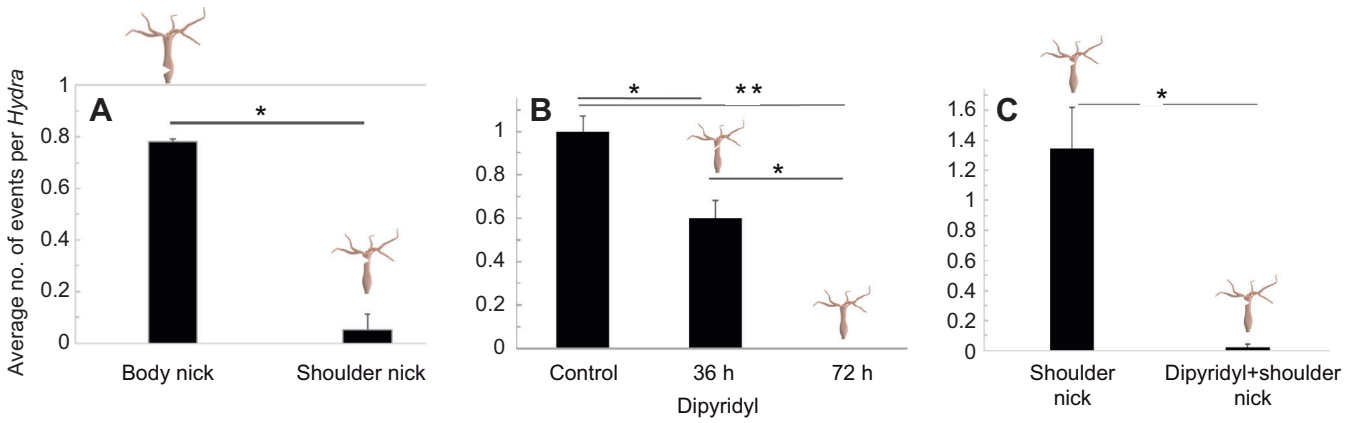

Fig. 6. The stiffness differential in the body column is essential for locomotion through the somersault. (A) The extracellular matrix was perturbed locally in *Hydra* polyps using a partial cut (nick), to abolish the stiffness differential. The graph shows the average number of somersault events per *Hydra* with nicks at the shoulder or the body column. The measurements were recorded 6 h after the manipulation. (B) The extracellular matrix was perturbed globally using the chemical disruption of collagens by treatment with 10 mmol l^{-1} dipyridyl. The average number of somersault events per *Hydra* was reduced upon treatment with dipyridyl for 36 h, and no events were observed after treatment with dipyridyl for 72 h. (C) The stiffness differential was perturbed by disrupting the extracellular matrix with a combination of dipyridyl treatment and a partial nick. As shown in the graph, this led to a reduction in the average number of somersault events observed compared with that for animals not treated with dipyridyl. In both cases, measurements were performed 36 h after treatment. For all the graphs, the error bars represent s.e.m., and the significance values are calculated using two-tailed Student's *t*-test (*P<0.05, **P<0.005; n=20 polyps per experiment, n=3 experiments). See also Table S4.

polyps per experiment, n=3 experiments). This confirmed the correlation of the degree of unpolymerized fibrillar collagen in the extracellular matrix with the inability to somersault. These observations suggest that the extracellular matrix-mediated stiffness differential in the *Hydra* polyp is crucial for somersaulting. In a third experiment, the animals with a lesion in the shoulder region were treated with dipyridyl, to prevent regeneration of the extracellular matrix in the nicked region. In this case, even 36 h after nicking, the polyps were unable to regain the ability to somersault (Fig. 6C; Movie 5).

To probe deeper into the role of tissue stiffness as a function of collagen crosslinking, we monitored the ultrastructure of the extracellular matrix in mesoglea using scanning electron microscopy (SEM). Tissue sections were prepared from the shoulder region and body column to reveal the difference, if any, in the ultrastructure of the extracellular matrix reflecting the tissue stiffness differential. SEM images of these sections revealed clear demarcation of the mesoglea, indicated in the dash–dot orange line separating the ectodermal tissue from endodermal tissue (Fig. 7). Within mesoglea, because of the transverse sectioning of the tissue, the central interstitial matrix consisting of fibrillar collagens was distinctly visible (Fig. 7A–D). In the control polyps, comparison of the SEM images clearly showed the differential packing of the extracellular matrix collagen fibers and indicated that this could be attributed to differential collagen crosslinking (Fig. 7A,B). These observations suggest that the stiffness differential observed between the shoulder region and body column was due to the differential packing of collagen fibers in the extracellular matrix. As discussed above, dipyridyl treatment of *Hydra* polyps resulted in the loss of differential stiffness between the shoulder and the body column by inhibiting crosslinking of the collagen fibers (Fig. S6B) at 72 h. To evaluate such an effect on the ultrastructure of the *Hydra* extracellular matrix, we monitored the extracellular matrix structure in polyps after dipyridyl treatment. We performed SEM imaging of tissue sections of dipyridyl-treated polyps in the shoulder region and body column. The polyps treated with dipyridyl for 72 h corroborated the results obtained through stiffness measurements using AFM (Fig. 7C,D,). Inhibition of lysyl oxidase activity by dipyridyl caused an extensive reduction in collagen crosslinking in the shoulder region (Fig. 7C) as compared with the control polyps. The extracellular matrix ultrastructure at the body column after dipyridyl treatment appeared unaffected relative to the control polyps. This observation also confirmed that collagen in the mesoglea of the body column is sparsely crosslinked as compared with that at the shoulder region. Collectively, these findings provide compelling evidence that spatial variation in tissue stiffness is a function of collagen crosslinking and is crucial for the somersault, corroborating the results of the simulations.

DISCUSSION

Using AFM measurements, we have obtained more definitive results following earlier reports of tissue stiffness in *Hydra* (Carter et al., 2016). Here, we demonstrated that *Hydra* possesses a local variation in tissue stiffness at a ratio of 3:1 between the shoulder region and the rest of the body column. To understand the significance of such a sharp stiffness differential in the body column, we investigated the seemingly strenuous process of somersaulting (Biewener, 1990). The simulations revealed that the observed differential in tissue stiffness has important consequences in terms of energy transfer to stand upside down. In congruence with simulations, the *Hydra* polyps lacking the stiffness differential were unable to stand upside down during somersault. Further, the differential stiffness of the body column enables efficient transfer of mechanical energy stored in stretching to bending. While somersaulting allows the polyp to move around in the immediate environment at intermediate distances, looping allows the polyps to cover smaller distances. For larger distance locomotion, floating using an air bubble seems more favorable. We also observed that the polyps showed a higher propensity to perform looping, somersaulting or stretching when we detached them and dropped them back into the culture bowl. This behavior can be explained by the need for *Hydra* to probe the immediate surroundings to gauge the nature of the new site. Such probing might be important in obtaining different information by the polyp, including water flow differential in the surroundings, better substrate attachment sites, prey abundance, etc.

Journal of Experimental Biology (2020) 223, jeb232702. doi:10.1242/jeb.232702

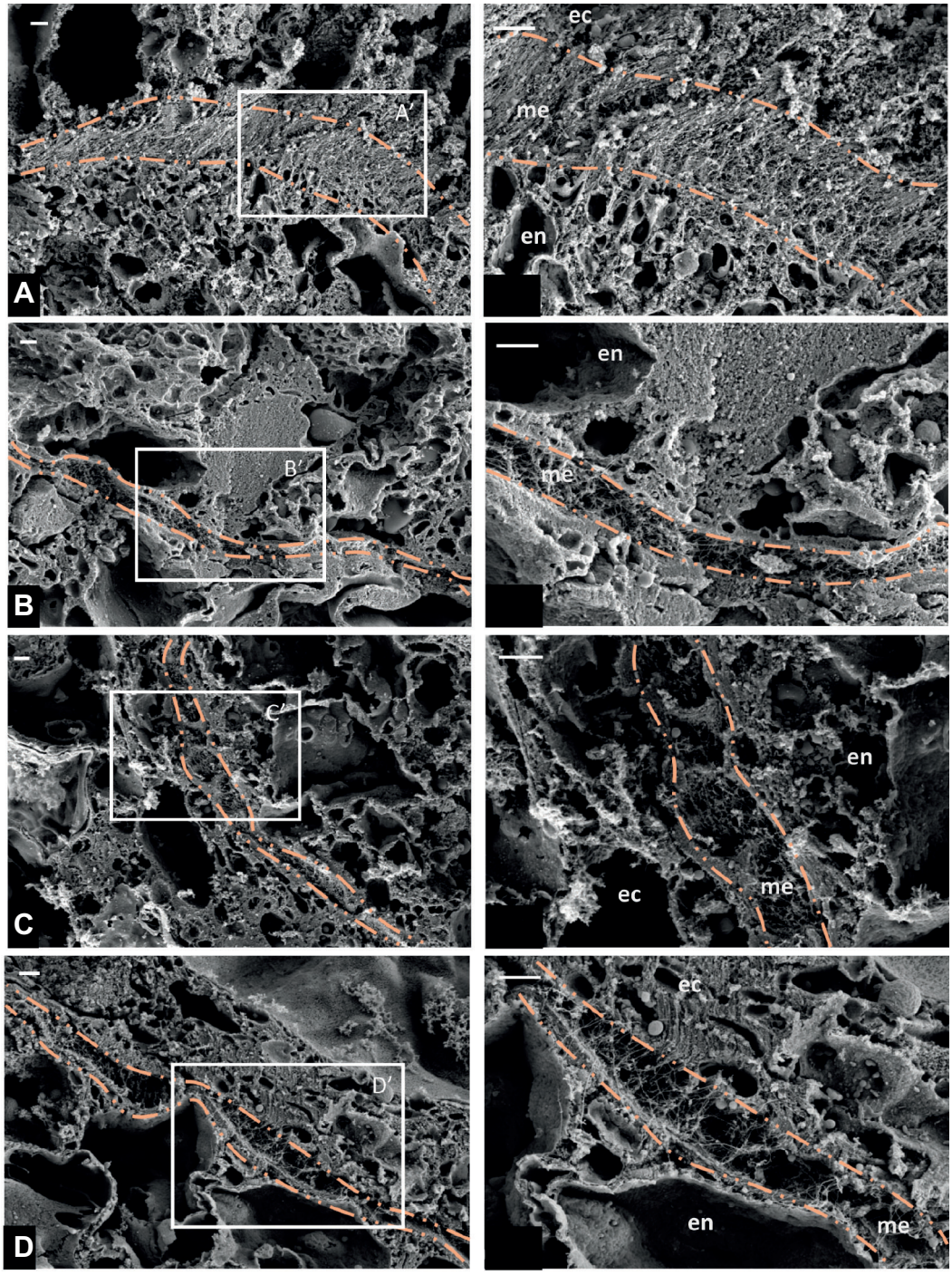

Fig. 7. Scanning electron micrographs (SEM) of *Hydra* mesoglea showing changes in the extracellular matrix between the shoulder region and body column following dipyridyl treatment. (A,B) Control, (C,D) dipyridyl-treated polyps. (A) SEM of mesoglea (dash–dot orange line) from the shoulder region of the control polyp in transverse section (TS) showing dense collagen fibers. (B) SEM image of mesoglea (dash–dot orange line) from the body column region of the control polyp in TS showing less dense collagen fibers. (C) SEM image of mesoglea (dash–dot orange line) from the shoulder region of the polyp after dipyridyl treatment for 72 h in TS, showing loosely packed collagen fibers as a result of inhibition of collagen crosslinking. (D) SEM image of mesoglea (dash–dot orange line) from the body column region of the polyp after dipyridyl treatment for 72 h in TS, showing loosely packed collagen fibers as a result of inhibition of collagen crosslinking. For A–D, a higher magnification image of the boxed region is shown on the right. Scale bars: 1 µm. ec, ectoderm; en, endoderm; me, mesoglea.

The arrangement of the shoulder and the body column can be compared to that of tendons and muscles in vertebrates. The shoulder region acts like a spring storing energy and repurposing it to lift vertically, similar to mechanisms proposed for motion during terrestrial walking (Markowitz and Herr, 2016; Taylor and Heglund, 1982). The tentacles allow for stability by providing lateral forces similar to insect legs (Dickinson et al., 2000). Energy recycling through tendons and other elastic elements is an established mechanism in locomotion in vertebrates such as humans (Cavagna et al., 1977). Tendons consist of thick bundles of

collagen fibers secreted by tenocytes. Incidentally, tenocytes can change the extracellular matrix composition of tendons in response to changes in mechanical loading and hence the elasticity (Hansen et al., 2009). Based on our study, mechanisms modulating elastic properties of tissues to facilitate locomotion seem to have evolved early in the animal phyla and hence this seems to be an ancient function of the extracellular matrix. It points to the possibility that shear stresses faced during tentacle movement as well as the structural peculiarities of the organism may have played a role in evolving the stiffness differential (Carter et al., 2016; Shostak et al., 1965; Haynes et al., 1968). The torsional forces for moving a flexible rod-like structure as a tentacle in water could be in the nanonewton/micronewton range and deformations in the hypostome would be responsible for producing these forces. Such scales of repetitive deformations could have led to the evolution of mechanosensory feedback mechanisms required for regulating the extracellular matrix stiffness. One of the easiest ways to achieve this is by modulating the crosslinking of fibrillar collagens in the extracellular matrix, an example of which we have illustrated here. The observed differential in tissue stiffness is possibly a harbinger in the evolution of a spatially heterogeneous stiffness of extracellular matrix which enables movement. A similar mechanism might have further evolved in more complex higher organisms during the development of the musculoskeletal system.

Our study underscores the importance of the observed changes in cellular and molecular properties at the shoulder region and their mechanistic contribution to the process of locomotion in *Hydra*. The cellular movement shows a marked difference between the shoulder region and the body column (Holstein et al., 1991). All the cells in a polyp are known to be pushed towards the termini of the body and sloughed off. The extracellular matrix associated with these cells is also reported to move along with these cells and is degraded at the tentacle tip or the basal disk (Aufschnaiter et al., 2011). Strangely, the aforesaid behavior changes at the shoulder region with a reduction in the cell–extracellular matrix velocities. This could be due to differential interactions of cells with the components of the extracellular matrix in the shoulder region versus the rest of the body column, as has been proposed earlier (Shostak et al., 1965). The extracellular matrix is degraded within the shoulder region rather than being pushed to the tentacles, indicating that the extracellular matrix in this region is maintained differently than the other regions. Further, BrdU staining indicates a cessation of the proliferative capacity of the stem cell as they cross the boundary towards the shoulder region and into the hypostome and tentacles (Reddy et al., 2015). In *Hydra*, the tentacles and the hypostome region possess a wide range of differentiated cells, which terminally differentiate as they move from the gastric region towards the hypostome and tentacles (Wood, 1979; Ewer and Fox, 1947). It would be interesting to study whether, similar to human and mice cells, stiffness properties of the extracellular matrix determine the differentiation fate of these cells in *Hydra* (Engler et al., 2006; Park et al., 2011). Thus, tissue stiffness in *Hydra* is innately linked not only to the motility of the organism but also possibly to other processes.

Collagen, as shown here, plays an important role in tissue stiffness, possibly both through cell–extracellular matrix interactions and varying extracellular matrix composition (Shostak et al., 1965; Aufschnaiter et al., 2011; Zhang et al., 2007; Shimizu et al., 2008; Sarras, 2012). The collagen fiber structure in the extracellular matrix can be dynamically regulated depending on the strain experienced locally (Haynes et al., 1968). Further studies need to be performed to understand how collagen and other extracellular matrix molecules are regulated along the oral–aboral axis of *Hydra*. Our findings not only open a new avenue in invertebrate locomotion mechanics, which could lead to interesting insights into the evolution of locomotion, but also lay a foundation for furthering mechanobiology in lower organisms using AFM-based measurements. Additionally, the need for an optimal elasticity variation for greater energy efficiency in liquid environments could be a significant design principle for building artificial machines and advance the field of untethered small-scale robots working in confined areas (Hu et al., 2018).

Acknowledgements
We wish to thank Dr Sudhakaran Prabhakaran and Dr Sanjay Sane for useful comments on the manuscript. We thank Yashodeep Matange and Kanchan Sharma for help with animations and Dr Arpita Roychoudhury, Jitesh Seth and Adarsh Kumar for assistance with experiments. The electron microscopy imaging was performed at the Irving and Cherna Moskowitz Center for Nano and Bio-Nano Imaging at the Weizmann Institute of Science, Rehovot, Israel.

Competing interests
The authors declare no competing or financial interests.

Author contributions
Conceptualization: S.A.N., M.K.U., P.R., I. Solomonov, A.C., S.P., S.G.; Methodology: S.A.N., M.K.U., D.S., S.S.R., E.K., S.P., S.G.; Software: D.S., A.C.; Validation: S.A.N., M.K.U., S.P., S.G.; Formal analysis: S.A.N., M.K.U., D.S.; Investigation: S.A.N., M.K.U.; Resources: E.K., I. Sagi, A.C., S.P., S.G.; Data curation: S.A.N., M.K.U., I. Solomonov, S.P., S.G.; Writing - original draft: S.A.N., M.K.U., A.C., S.P., S.G.; Writing - review & editing: S.A.N., M.K.U., P.R., A.C., S.P., S.G.; Visualization: S.A.N., M.K.U., D.S., E.K.; Supervision: I. Sagi, A.C., S.P., S.G.; Project administration: I. Sagi, S.P., S.G.; Funding acquisition: I. Sagi, S.G.

Funding
This work was supported by the Centre of Excellence in Epigenetics program (BT/01/COE/09/07) of the Department of Biotechnology, Government of India and the JC Bose National Fellowship from the Science and Engineering Research Board (JCB/2019/000013) (S.G.). We used the computer cluster obtained using a grant from the Department of Biotechnology (BT/PR16542/BID/7/654/2016) to A.C. A.C. acknowledges funding by DST Nanomission, India, the Thematic Unit Program (SR/NM/TP-13/2016) and the Department of Science and Technology, India (MTR/2019/000078). The authors acknowledge funding from IISER Pune - intramural (D.S., S.S.R., S.G., S.P. and A.C.); Department of Biotechnology postdoctoral fellowship (PCR); the Wellcome Trust-Department of Biotechnology India Alliance for Intermediate Fellowship (500172/Z/09/Z) (S.P.) and Early Career Fellowship (IA/E/16/1/503057) (P.C.R.); Department of Science and Technology, India (SERB grant no. EMR/2015/000018; A.C.); fellowships from the University Grants Commission (UGC) (M.U.); EMBO Short-term fellowship and Infosys Foundation for international travel support (M.U.); and Kishore Vaigyanik Protsahan Yojana (KVPY) (S.N.).

Data availability
Source data files are available from the Dryad Digital Repository (Naik et al., 2020): https://doi.org/10.5061/dryad.qbzkh18fx

Supplementary information
Supplementary information available online at
https://jeb.biologists.org/lookup/doi/10.1242/jeb.232702.supplemental

References
Akhtar, R., Sherratt, M. J., Cruickshank, J. K. and Derby, B. (2011). Characterizing the elastic properties of tissues. *Mater. Today* **14**, 96-105. doi:10.1016/S1369-7021(11)70059-1

Alexander, R. M. (2003). *Principles of Animal Locomotion*. Princeton University Press.

Anderson, E. J. and Demont, M. E. (2000). The mechanics of locomotion in the squid Loligo pealei: locomotory function and unsteady hydrodynamics of the jet and intramantle pressure. *J. Exp. Biol.* **203**, 2851-2863.

Aufschnaiter, R., Zamir, E. A., Little, C. D., Özbek, S., Münder, S., David, C. N., Li, L., Sarras, M. P. and Zhang, X. (2011). In vivo imaging of basement membrane movement: ECM patterning shapes Hydra polyps. *J. Cell Sci.* **124**, 4027-4038. doi:10.1242/jcs.087239

Aufschnaiter, R., Wedlich-Söldner, R., Zhang, X. and Hobmayer, B. (2017). Apical and basal epitheliomuscular F-actin dynamics during Hydra bud evagination. *Biol. Open* **6**, 1137-1148. doi:10.1242/bio.022723

Barnes, H. A., Hutton, J. F. and Walters, K. (1989). *An Introduction to Rheology*, Vol. 3. Elsevier.
Biewener, A. A. (1990). Biomechanics of mammalian terrestrial locomotion. *Science* **250**, 1097-1103. doi:10.1126/science.2251499
Bode, H. R. (1996). The interstitial cell lineage of hydra: a stem cell system that arose early in evolution. *J. Cell Sci.* **109**, 1155-1164.
Bode, H. R., Gee, L. W. and Chow, M. A. (1990). Neuron differentiation in hydra involves dividing intermediates. *Dev. Biol.* **139**, 231-243. doi:10.1016/0012-1606(90)90292-Q
Bond, C. and Harris, A. K. (1988). Locomotion of sponges and its physical mechanism. *J. Exp. Zool.* **246**, 271-284. doi:10.1002/jez.1402460307
Bray, D. (2000). *Cell Movements: From Molecules to Motility*. Garland Science.
Carter, J. A., Hyland, C., Steele, R. E. and Collins, E.-M. S. (2016). Dynamics of mouth opening in Hydra. *Biophys. J.* **110**, 1191-1201. doi:10.1016/j.bpj.2016.01.008
Cavagna, G. A., Heglund, N. C. and Taylor, C. R. (1977). Mechanical work in terrestrial locomotion: two basic mechanisms for minimizing energy expenditure. *Am. J. Physiol. Regul. Integr. Comp. Physiol.* **233**, R243-R261. doi:10.1152/ajpregu.1977.233.5.R243
Davis, L. E., Burnett, A. L., Haynes, J. F., Osborne, D. G. and Spear, M. L. (1968). Histological and ultrastructural study of the muscular and nervous systems in Hydra. II. Nervous system. *J. Exp. Zool.* **167**, 295-331. doi:10.1002/jez.1401670305
Deutzmann, R., Fowler, S., Zhang, X., Boone, K., Dexter, S., Boot-Handford, R., Rachel, R. and Sarras, M. (2000). Molecular, biochemical and functional analysis of a novel and developmentally important fibrillar collagen (Hcol-I) in hydra. *Development* **127**, 4669-4680.
Dhont, J. K. (1996). *An Introduction to Dynamics of Colloids*: Elsevier.
Dickinson, M. H., Farley, C. T., Full, R. J., Koehl, M., Kram, R. and Lehman, S. (2000). How animals move: an integrative view. *Science* **288**, 100-106. doi:10.1126/science.288.5463.100
Dupre, C. and Yuste, R. (2017). Non-overlapping neural networks in Hydra vulgaris. *Curr. Biol.* **27**, 1085-1097. doi:10.1016/j.cub.2017.02.049
Engler, A. J., Sen, S., Sweeney, H. L. and Discher, D. E. (2006). Matrix elasticity directs stem cell lineage specification. *Cell* **126**, 677-689. doi:10.1016/j.cell.2006.06.044
Ewer, R. and Fox, H. M. (1947). On the Functions and Mode of Action of the Nematocysts of Hydra. Proceedings of the Zoological Society of London. Wiley Online Library, 365-376.
Galliot, B. (2000). Conserved and divergent genes in apex and axis development of cnidarians. *Curr. Opin. Genet. Dev.* **10**, 629-637. doi:10.1016/S0959-437X(00)00141-6
Gemmell, B. J., Colin, S. P., Costello, J. H. and Dabiri, J. O. (2015). Suction-based propulsion as a basis for efficient animal swimming. *Nat. Commun.* **6**, 1-8. doi:10.1038/ncomms9790
Gray, J. (1933). Studies in animal locomotion: I. The movement of fish with special reference to the eel. *J. Exp. Biol.* **10**, 88-104.
Han, S., Taralova, E., Dupre, C. and Yuste, R. (2018). Comprehensive machine learning analysis of Hydra behavior reveals a stable basal behavioral repertoire. *eLife* **7**, e32605. doi:10.7554/eLife.32605
Hansen, P., Hassenkam, T., Svensson, R. B., Aagaard, P., Trappe, T., Haraldsson, B. T., Kjaer, M. and Magnusson, P. (2009). Glutaraldehyde cross-linking of tendon—mechanical effects at the level of the tendon fascicle and fibril. *Connect. Tissue Res.* **50**, 211-222. doi:10.1080/03008200802610040
Haynes, J. F., Burnett, A. L. and Davis, L. E. (1968). Histological and ultrastructural study of the muscular and nervous systems in Hydra. I. The muscular system and the mesoglea. *J. Exp. Zool.* **167**, 283-293. doi:10.1002/jez.1401670304
Holstein, T. W., Hobmayer, E. and David, C. N. (1991). Pattern of epithelial cell cycling in hydra. *Dev. Biol.* **148**, 602-611. doi:10.1016/0012-1606(91)90277-A
Hu, W., Lum, G. Z., Mastrangeli, M. and Sitti, M. (2018). Small-scale soft-bodied robot with multimodal locomotion. *Nature* **554**, 81-85. doi:10.1038/nature25443
Lenhoff, H. (2013). *Hydra: Research Methods*: Springer Science & Business Media.
Markowitz, J. and Herr, H. (2016). Human leg model predicts muscle forces, states, and energetics during walking. *PLoS Comput. Biol.* **12**, e1004912. doi:10.1371/journal.pcbi.1004912
Martínez, D. E., Iñiguez, A. R., Percell, K. M., Willner, J. B., Signorovitch, J. and Campbell, R. D. (2010). Phylogeny and biogeography of Hydra (Cnidaria: Hydridae) using mitochondrial and nuclear DNA sequences. *Mol. Phylogenet. Evol.* **57**, 403-410. doi:10.1016/j.ympev.2010.06.016
Matsumoto, G. (1991). Swimming movements of ctenophores, and the mechanics of propulsion by ctene rows. *Hydrobiologia* **216**, 319-325. doi:10.1007/BF00026481
Naik, S. A., Unni, M. K., Sinha, D., Rajput, S. S., Reddy, P. C., Kartvelishvily, E., Solomonov, I., Sagi, I., Chatterji, A., Patil, S. et al. (2020). Differential tissue stiffness of body column facilitates locomotion of *Hydra* on solid substrates, v3. Dryad, Dataset, doi:10.5061/dryad.qbzkh18fx
Park, J. S., Chu, J. S., Tsou, A. D., Diop, R., Tang, Z., Wang, A. and Li, S. (2011). The effect of matrix stiffness on the differentiation of mesenchymal stem cells in response to TGF-β. *Biomaterials* **32**, 3921-3930. doi:10.1016/j.biomaterials.2011.02.019
Reddy, P. C., Barve, A. and Ghaskadbi, S. (2011). Description and phylogenetic characterization of common hydra from India. *Curr. Sci.* **101**, 736-738.
Reddy, P. C., Unni, M. K., Gungi, A., Agarwal, P. and Galande, S. (2015). Evolution of Hox-like genes in Cnidaria: study of Hydra Hox repertoire reveals tailor-made Hox-code for cnidarians. *Mech. Dev.* **138**, 87-96. doi:10.1016/j.mod.2015.08.005
Roberts, T. J. (2016). Contribution of elastic tissues to the mechanics and energetics of muscle function during movement. *J. Exp. Biol.* **219**, 266-275. doi:10.1242/jeb.124446
Sarras, M. P., Jr (2012). Components, structure, biogenesis and function of the Hydra extracellular matrix in regeneration, pattern formation and cell differentiation. *Int. J. Dev. Biol.* **56**, 567-576. doi:10.1387/ijdb.113445ms
Sarras, M. P., Jr, Meador, D. and Zhang, X. (1991). Extracellular matrix (Mesoglea) of Hydra vulgaris: II. Influence of collagen and proteoglycan components on head regeneration. *Dev. Biol.* **148**, 495-500. doi:10.1016/0012-1606(91)90267-7
Shimizu, H., Zhang, X., Zhang, J., Leontovich, A., Fei, K., Yan, L. and Sarras, M. P. (2002). Epithelial morphogenesis in hydra requires de novo expression of extracellular matrix components and matrix metalloproteinases. *Development* **129**, 1521-1532.
Shimizu, H., Aufschnaiter, R., Li, L., Sarras, M. P., , Jr, Borza, D.-B., Abrahamson, D. R., Sado, Y. and Zhang, X. (2008). The extracellular matrix of hydra is a porous sheet and contains type IV collagen. *Zoology* **111**, 410-418. doi:10.1016/j.zool.2007.11.004
Shostak, S., Patel, N. G. and Burnett, A. L. (1965). The role of mesoglea in mass cell movement in Hydra. *Dev. Biol.* **12**, 434-450. doi:10.1016/0012-1606(65)90008-4
Siegel, R. C., Pinnell, S. R. and Martin, G. R. (1970). Cross-linking of collagen and elastin. Properties of lysyl oxidase. *Biochemistry* **9**, 4486-4492. doi:10.1021/bi00825a004
Tao, N. J., Lindsay, S. M. and Lees, S. (1992). Measuring the microelastic properties of biological material. *Biophys. J.* **63**, 1165. doi:10.1016/S0006-3495(92)81692-2
Taylor, C. R. and Heglund, N. C. (1982). Energetics and mechanics of terrestrial locomotion. *Annu. Rev. Physiol.* **44**, 97-107. doi:10.1146/annurev.ph.44.030182.000525
Trembley, A. (1744). *Mémoires pour servir à l'histoire d'un genre de polypes d'eau douce, à bras en forme de cornes*. Chez Jean & Herman Verbeek.
Wood, R. L. (1979). The fine structure of the hypostome and mouth of hydra. *Cell Tissue Res.* **199**, 319-338. doi:10.1007/BF00236142
Zhang, X., Boot-Handford, R. P., Huxley-Jones, J., Forse, L. N., Mould, A. P., Robertson, D. L., Athiyal, M. and Sarras, M. P. (2007). The collagens of hydra provide insight into the evolution of metazoan extracellular matrices. *J. Biol. Chem.* **282**, 6792-6802. doi:10.1074/jbc.M607528200